Chapter 4 Results and discussions

4.1 Effects of catalyst thickness on CNTs growth

Figures 4-1 (a), (b) and (c) show the top view SEM images of 100 nm Co-assisted CNTs grown with H_2/CH_4 ratio of 10/20, 10/10 and 20/10 sccm/sccm for Specimens A1, A2 and A3, respectively. Figures 4-1 (d), (e) and (f) depict the top view SEM images of 150 nm Co-assisted CNTs grown with H_2/CH_4 ratio of 10/20, 10/10 and 20/10 sccm/sccm for Specimens B1, B2 and B3, respectively. The corresponding side view SEM images of Fig. 4-1 are shown in Fig. 4-2. The detailed deposition conditions and the features of CNTs are listed in Tables 3-1 and 4-1, respectively. The results show that the morphologies of CNTs can be mainly divided into two groups: tubule-like and rattan-like.

By comparing the tubule-like CNTs synthesized under different catalyst thicknesses, the results also indicate that the CNTs grown under low catalyst thickness are generally with smaller diameter and higher tube number density, where the smallest diameter is about 80 nm, and the highest tube number density can go up to 3.89 Gtube/inch^2, as indicated for Specimen A3 in Table 4-1. This is in agreement with the reported statements in the literatures [Qin 98-3437; Wei 01-1394]: a thinner catalyst film can be melted and reduced by H-plasma pretreatment to become a lot of smaller and denser activated islands, which act as the catalyst to absorb carbon element from the gas phase and then carbon element diffuse and precipitate to form CNTs. Therefore, the diameter of CNTs is closely associated with the size of the catalyst particles. The diameter and tube number density can be manipulated by adjusting the catalyst thickness.

4.2 Effects of H_2 and CH_4 flow rates on CNTs growth

By comparing the Specimens A1 and A2 in Table 4-1, the morphologies of CNTs can be varied from rattan-like to partial tubule-like appearance by changing CH_4 flow rate from 20 to 10 sccm, as compared Figs. 4.2 (a) with (b). It seems to indicate that too high in carbon source concentration is not a favor condition to grow tubule-like CNTs. Carbon from the gas phase may be consumed by three main paths, i.e., (1) absorbed into one side of the catalyst and precipitate on other side to form CNTs, (2) deposit on the catalyst sides during CNTs growth, and (3) etched off by H-plasma. Therefore, an overabounding carbon concentration in the gas

phase is a more favor condition for continuously depositing on the sides of catalysts. Thus, the rattan-like CNTs take shape. On the other hand, an increase in hydrogen flow rate is essentially to etch off more deposited carbon on the catalyst sides, which is a favor condition to form tubule-like CNTs. This is in agreement with the present results by comparing the CNTs images in Specimens A2 with A3 (Figs. 4-2(b) with (c)). Same conclusions on effects of H_2 and CH_4 concentrations can also be drawn from Specimens B1, B2 and B3 (Figs. 4-2 (d), (e) and (f)).

In conclusion, CH_4 and H_2 concentrations play a crucial role to determine the CNTs morphology, which act as the carbon source and etchant, respectively. The formation of rattan-like CNTs can be suppressed by decreasing CH_4 or increasing H_2 flow rate.

4.3 H-plasma and chemical etching post treatment for the open-ended CNTs

The post-treatments are a combination of H-plasma treatment and chemical etching of different processing times, as shown in Table 3-2. Morphology of the as-grown rattan-like CNTs for Specimen B1 is shown in Fig. 4-2 (d). The corresponding top and side view morphologies of the H-plasma post-treated CNTs for 1 to 7 min etching time are depicted in Figs. 4-3(a) ~ (f). The results indicate that the carbon sheets of the rattan-like CNTs (Specimen B1) can be gradually etched off by increasing etching time and the CNTs themselves may be finally destructed. This is in agreement with effect of H_2 flow rate on CNTs growth, where H-plasma can act as an etchant, as discussed in the previous paragraph. The results also imply that after intermediate 7 min H-plasma treatment time, the rattan-like CNTs will become tubule-like CNTs without apparent structure damage (Fig. 4-3 (f)). In other words, the CNTs after 7 min H-plasma post-pretreatment can still maintain their structure integrity.

The top and side view morphologies of the 7 min H-plasma post-treated CNTs after further etching by HNO_3 for 3 min are shown in Figs. 4-4 (a) and (b), respectively. It shows that catalyst particles are removed chemically owing to the chemical reaction as below [http://chemwww.pu.] :

$$Co_{(s)} + 4HNO_{3\,(aq)} \rightarrow 2H_2O_{(l)} + 2Co(NO_3)_{2(aq)} + 2NO_{2(g)}$$

Thus it can be seen the rattan-like tubes can be cleaned by H-plasma and the catalyst by HNO_3 to become open-ended tubes via this proposing post-treatment process. As mentioned above, in the case of insufficient H_2 or overabounding CH_4 content, it can lead to the formation of the

rattan-like CNTs. The post-treatment provides a remedial method to change CNTs morphology from rattan-like to tubule-like or further tubule-like CNTs with the opened-tips.

In order to realize the detailed effects of post-treatment on nanostructures of the as-grown CNTs, the tubule-like CNTs (Specimen C1) was chosen to be post-treated. The SEM and TEM morphologies of tubule-like CNTs (Specimen C1) are shown in Figs. 4-5 (a) and (b), respectively. It displays the tip catalyst particles of the highly aligned tubes are covered by ultra-thin carbon layers about 3 ~ 5 nm in thickness. The corresponding SEM morphologies of the H-plasma post-treated CNTs for 1, 4, 7 and 10 min etching times are shown in Figs. 4-6 (a) ~ (d), respectively. Similar to effect of H-plasma on the rattan-like CNTs, the tubule-like CNTs can be gradually become sparser in tube number density, partial open-ended tips and finally be destructed. Furthermore, it is noted that the CNTs can still maintain their structure integrity with removal of C layers on the catalyst surface after 1 min etching time, as shown in TEM image of Fig. 4-7. However, after 10 min etching time, the structure integrity of the stems of CNTs is almost seriously damaged, as shown in TEM image of Fig. 4-8. In order to study effect of chemical etching post-treatment on CNTs structures, experiments were conducted to examine the possibility of direct chemical etching without prior H-plasma post-treatment on the as-grown CNTs. It was found that direct chemical etching to remove catalysts is very difficult due to carbon layers protection on the catalyst surface. Therefore, before chemical etching, one minute H-plasma post-treatment is a required step to etch off the carbon layers without damaging the stems of CNTs.

On effects of H-plasma plus chemical etching post-treatment, Figs. 4-9 (a) and (b) show the SEM morphologies of post-treated tubule-like CNTs (Specimen C1), which were etched by H-plasma for 1 min and immersed in 0.25 M HNO_3 for 2 and 3 min (Con. 2 and 3), respectively. The corresponding TEM micrographs of Figs. 4-9 (a) and (b) are shown in Figs. 4-10 (a) and (b), respectively. It presents that at least, chemical etching time of 3 min is required to entirely remove the catalyst from CNTs tips. In conclusion, to fabricate the open-ended CNTs, a two-step post-treatment of a 1 min H-plasma process and a 3-min 0.25 M HNO_3 etching step is required, which is capable to maintain the structure integrity of CNTs and to remove the catalysts completely.

4.4 Mechanism of H-plasma post-treatment

Regarding the anisotropic etching features of H-plasma on CNTs, Ajayan's group

proposed that the presence of pentagonal carbon ring at strained region on CNTs tips makes them more active than the cylindrical tubes which are nearly composed of hexagonal network. On anisotropic reaction in oxygen atmosphere, Kung, et al. suggested the highly strained CNTs end tips will be earlier oxidized than the less strained side walls of CNTs (Ref. to Section 2.3.1) [Kung 02-4819]. By comparing Fig. 4-5 (b) with Fig. 4-7, the results conform to the above statements. The arrows in Fig. 4-5 (b) mark the strained regions with the greatest curvature on the as-grown CNTs tips, which are the preferred etched sites marked by the arrows in Fig. 4-7. For this reason, the removal of carbon layers on CNTs tips without damaging the stems of CNTs by H-plasma may greatly change the tip morphologies due to anisotropic etching effect. A careful control of the H-plasma post-treatment parameters is required to obtain the favor conditions for subsequent processes, which is an important pretreatment step before chemical etching to remove the catalysts from the CNTs tips.

4.5 Structure and composition variations by high temperature tip trimming

As shown in Fig. 4-10 (b), the tips of open-ended CNTs perform a bowl-like shape. Therefore, it was expected that the sites of bowl-like tips could be covered with more material than the side walls of CNTs. In order to cover the opened-tips with phase-change alloy, the open-ended CNTs were coated a $Ge_2Sb_2Te_5$ layer of 200 nm in thickness via sputtering process (Images of open-ended CNTs before and after alloy sputtering are illustrate in Figs. 4-9 (b), and 4-11 (a), respectively). Then, the sample was subsequently heated to 400 ℃, 420 ℃ and 440 ℃ in the vacuum range about 10^{-4} Torr for 30 minutes as shown in Figs. 4-11 (b), (c) and (d), respectively. It implies the phase-change alloy can be evaporated away at high temperature in vacuum.

The corresponding TEM images of Figs. 4-11 (b), (c) and (d) are shown in Figs. 4-12, 4-13 and 4-14, respectively. The results depict that the alloy can mostly survive on CNTs tips, and less on side walls of CNTs after heated at 420℃ for 30 min. It is speculated that the alloy sputtering direction was parallel to the tube axis may lead to the different deposition thickness on opened-tips and side walls of CNTs. The bowl-like opened-tips are the favor sites to be deposited more alloy material than the side walls of CNTs. Therefore, the alloy material deposited on side walls of CNTs can be quicker evaporated away.

As shown in Fig. 4-13, the upper right insert displayed the corresponding SAED pattern of the residual alloy on CNTs tip. On the basis of this experimental finding, the residual phase-change alloy performs a crystalline state. The corresponding Auger spectra of residual phase-change alloy on CNTs tips (400℃ and 420℃ for 30 min) are displayed in Fig. 4-15. The results represent only one element of $Ge_2Sb_2Te_5$, i.e. Ge can be clearly detected. The reason may be due to the different evaporation rate of elements. As shown in Table 2-1, it depicts the element, Ge, has higher melting point (T_m = 937.4℃) and heat of vaporization (H_v = 330 J/mole) than Sb (T_m = 630.9℃, H_v = 77.14 J/mole) and Te (T_m = 449.65℃, H_v = 52.55 J/mole). Therefore, it is speculated the elements, Sb and Te, are more easily evaporated away than Ge, leading to the composition alteration of phase-change alloy. On the other hand, the Auger signal of Sn is observed, it is speculated the presence of Sn signal may owing to the residual pollution in the sputtering chamber.

In conclusion, material can be capped on the opened-tips of CNTs by the above proposed processes. However, it may suffer a drawback of composition alternation of alloy. Therefore, the next important issue is to design a series of developed processes, which can both cap CNTs with alloy and maintain the alloy composition.

4.6 Raman spectra of CNTs

The Raman spectra of Specimens A1 ~ A3, B1 ~ B3 are shown in Figs. 4-16 (a) ~ (c) and 4-17 (a) ~ (c), respectively. Two sharp peaks approximately at 1330 and 1602 cm^{-1} are detected and identified as the D-band and G-band, respectively. The relative integrated intensity ratio of the two sharp peaks (I_D/I_G) is characterized as degree of graphitization.

The Raman I_D/I_G ratios of above-mentioned specimens are listed in Table 4-1. By comparing the bonding structure of CNTs grown with different H_2/CH_4 ratio, the results coincide with a reported statement [Tsai 01-P.47]: Amorphous carbon can be etched off and the CNTs can be purified by higher H-plasma concentration. Therefore, the higher H-plasma concentration can lead to the lower I_D/I_G ratios and more tubule-like CNTs formation.

4.7 CNTs morphology versus field emission property

According to the reported field emission microscopy (FEM) analysis, emission current is extracted from the CNTs tip [Kuzumaki 01-3699], i.e., only the last atoms in the C-C chain at CNTs

end participates in field emission phenomenon. Thus it can be seen the tip structure determines the field emission properties [Wang 01-4028]. In this section, the field emission analysis will be discussed for as-grown CNTs (Specimen C1), and CNTs post-treated by Cons. 1, 3 and 7. The results of J-E plots and corresponding F-N plots are shown in Figs. 4-18 (a) and (b), respectively. Curves 1, 2, 3 and 4 mean the field emission curves of as-grown CNTs, carbon layer-stripped CNTs, open-ended CNTs, and destructed open-ended CNTs, respectively. Good field emission performance for emitters generally means they simultaneously exhibit lower turn on voltage and higher current density. It shows that their turn on voltages (at 0.01 mA/cm^2) vary from 7.11 to more than 10 V/ m (value in Curve 4 > Curve 2 > Curve 1 > Curve3); the current density (at 10 V/ m) changes from 2.77 ×10^{-3} to 6.73 ×10^{-2} mA/cm^2 (value in Curve 3 > Curve 1 > Curve 2 > Curve 4).

It is suggested the four decisive factors such as aspect ratio, oxidation, structure integrity and tube number density, are responsible for the different emission performance as noted later. First, there are few proposed mechanisms about the reason for open-ended CNTs exhibiting better field emission performance than the as-grown CNTs [Chung 01-73; Kung 02-4819]. Moreover, Saito's group examined in situ by FEM that the field emission images of the open-ended CNTs represent a ring pattern [Saito 97-554]. It means that emission current is extracted from the ultra-sharp ring tips of the open-ended CNTs. By comparing Fig. 4-5 (b) with Fig. 4-10 (b), the open-ended CNTs have higher local aspect ratio on their opened bowl-like tips than the tips of as-grown CNTs, therefore the open-ended CNTs can exhibit better field emission performance. Furthermore, compare morphologies of as-grown CNTs (Specimen C1, Fig. 4-5(b)) with carbon layer-stripped CNTs (Fig. 4-7), the former exhibits higher emission current and lower turn on voltage than the latter, as shown in Table 4-3, Curves 1 and 2 in Fig. 4-18(a). It is speculated the surface of Co particles can be oxidized and just like an insulated Co particles which may interfere with electron tunneling effect, and therefore electrons are more difficult to be extracted from CNTs tips. On the other hand, H-plasma post-treatment may also cause a decrease in field emission properties by forming more defects and flatten surfaces at the tips. In other words, oxidation of catalyst, formation of defects and flatten surface on catalyst surface may be responsible for decreasing in emission properties. Finally, as shown in Fig. 4-6 (d) (CNTs etched by H-plasma for 10 min, Con. 7), it depicts the as-grown CNTs tips are removed, but it confusingly exhibit the worst field emission properties. In this case, the bad field emission performance may be due to a decrease in tube number density and destruction in structure integrity (Ref. to Figs. 4-6 (d) and 4-8). Base on the results, directly opening CNTs

tips by H-plasma post-treatment is not a favor condition to fabricate the CNTs field emission properties. Nevertheless, through the proper controlled two-step process includes hydrogen plasma and chemical etching, the open-ended CNTs with well structure integrity can be obtained. Above all, the as-grown CNTs can be enhanced their field emission ability via this proposed two-step post-treatment.

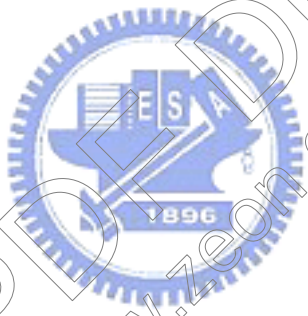

Table 4-1 Morphologies and bonding structures of various CNTs.

Specimen designation	Diameter (nm)	Tube number density (Gtube/inch^2)	CNTs morphology (as-grown)	I_D/I_G	Remarks
A1	-	-	Rattan-like	1.69	Figs. 4-1 (a) and 4-2 (a)
A2	~ 90	~ 3.52	Partial tubule-like	1.52	Figs. 4-1 (b) and 4-2 (b)
A3	~80	~ 3.89	Tubule-like	1.23	Figs. 4-1 (c) and 4-2 (c)
B1	-	-	Rattan-like	1.98	Figs. 4-1 (d) and 4-2 (d)
B2	~ 120	~ 2.99	Partial tubule-like	1.69	Figs. 4-1 (e) and 4-2 (e)
B3	~150	~ 2.67	Tubule-like	1.45	Figs. 4-1 (f) and 4-2 (f)

Table 4-2 Morphologies of the as-grown and post-treated CNTs.

Specimen designation		B1	C1
As-grown morphology (Fig. No.)		Rattan-like (4-1 (d),4-2 (d))	Tubule-like (4-5 (a), (b))
Post-treated morphology (Fig. No.)	Con. 1	Partial rattan-like (4-3 (a), (b))	Tubule-like CNTs without tip C layers (4-6 (a), (b))
	Con. 2	-	CNTs with partially removed catalyst (4-8 (a), (b))
	Con. 3	-	Open-ended CNTs (4-7 (a), (b))
	Con. 4	Partial tubule-like (4-3 (c), (d))	-
	Con. 5	Tubule-like (4-3 (e), (f))	-
	Con. 6	Open-ended CNTs (4-4 (a), (b))	-
	Con. 7	-	Destructed open-ended CNTs (4-9 (a), (b))

Table 4-3 Field emission properties and feature of CNTs for Specimen C1 after different post-treatment conditions.

Post treatment condition	Tube number density (Gtube/inch^2)	Field emission performance		Remarks
		Turn on field* (V/ m)	Current density# (mA/cm^2)	
Without post treatment	~2.25	8.65	3.17×10^{-2}	Figs. 4-5 (a), (b)
Con. 1	~2.14	9.72	1.30×10^{-2}	Figs. 4-6 (a), (b)
Con. 3	~2.08	7.11	6.73×10^{-2}	Figs. 4-7 (a), (b)
Con. 7	~1.49	> 10	2.77×10^{-3}	Figs. 4-9 (a), (b)

*Turn on field represents the value of voltage at emission current density = 0.01 mA/cm^2.
#Current density represents the value of emission current density at applied field = 10 V/ m

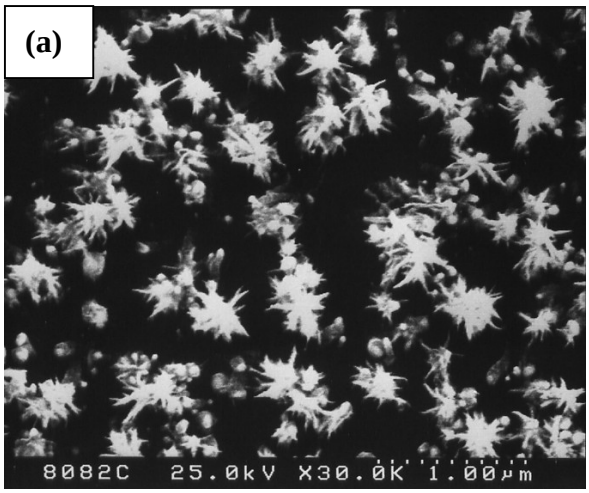

Specimen A1 (H_2/CH_4 : 10/20 sccm/sccm**)**

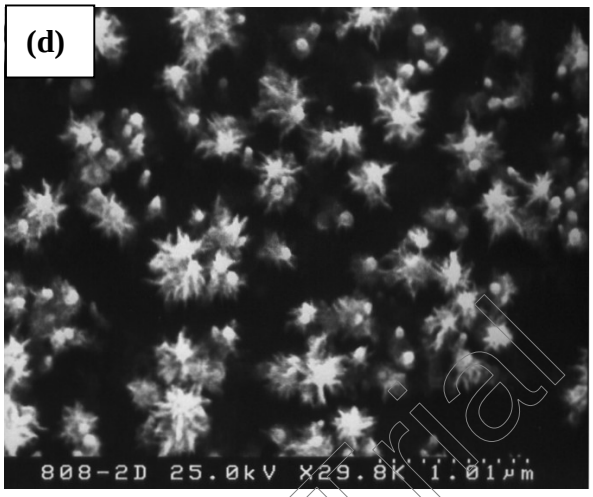

Specimen B1 (H_2/CH_4 : 10/20 sccm/sccm**)**

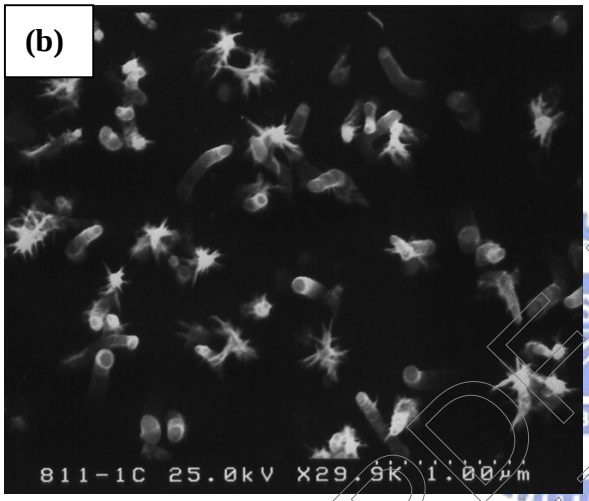

Specimen A2 (H_2/CH_4 : 10/10 sccm/sccm**)**

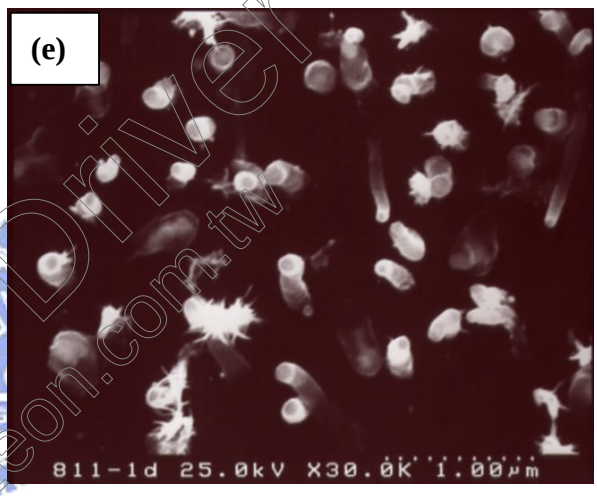

Specimen B2 (H_2/CH_4 : 10/10 sccm/sccm**)**

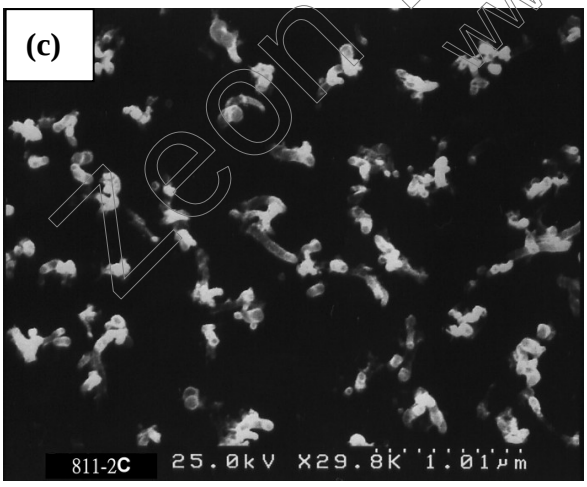

Specimen A3 (H_2/CH_4 : 20/10 sccm/sccm**)**

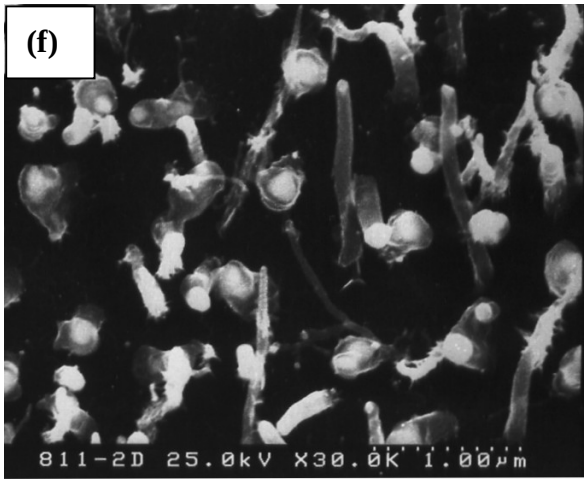

Specimen B3 (H_2/CH_4 : 20/10 sccm/sccm**)**

Figs. 4-1 Effect of H_2/CH_4 ratio (sccm/sccm) and catalyst thickness on CNTs morphology. (a), (b) and (c) are 100 nm Co-assisted CNTs grown with H_2/CH_4 ratio = 10/20, 10/10 and 20/10, respectively. (d), (e) and (f) are 150 nm Co-assisted CNTs grown with H_2/CH_4 ratio = 10/20, 10/10 and 20/10, respectively.

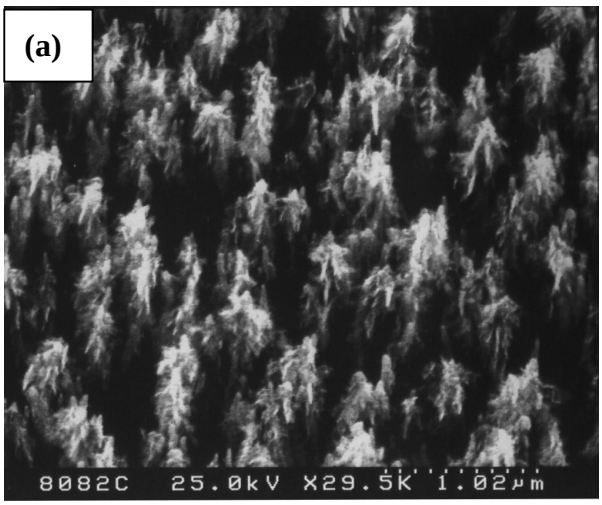

Specimen A1 (H_2/CH_4 : 10/20 sccm/sccm**)**

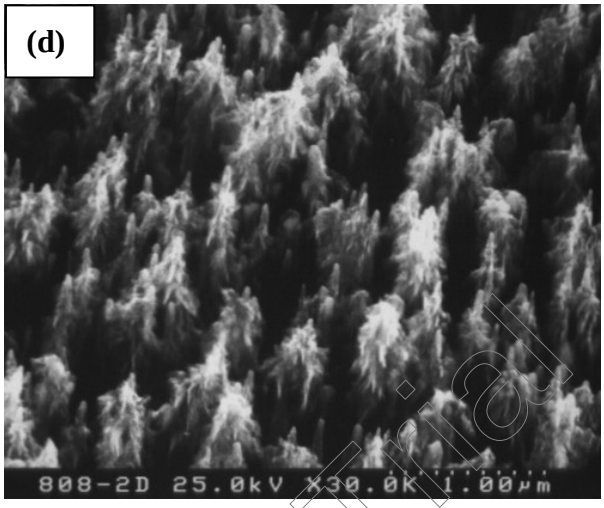

Specimen B1 (H_2/CH_4 : 10/20 sccm/sccm**)**

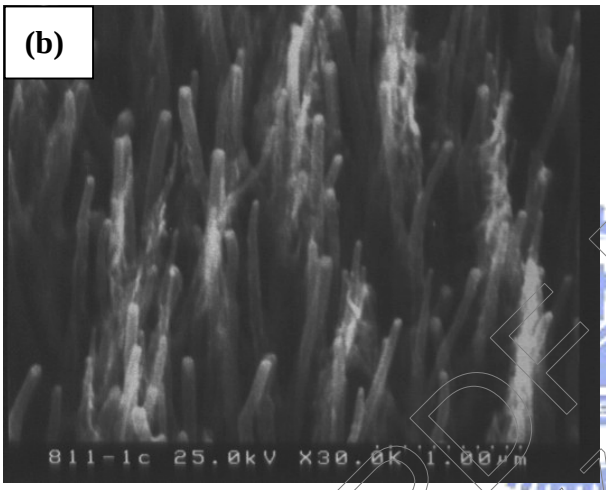

Specimen A2 (H_2/CH_4 : 10/10 sccm/sccm**)**

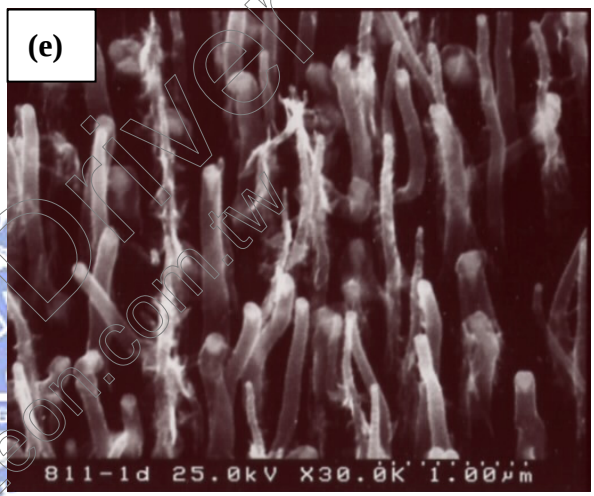

Specimen B2 (H_2/CH_4 : 10/10 sccm/sccm**)**

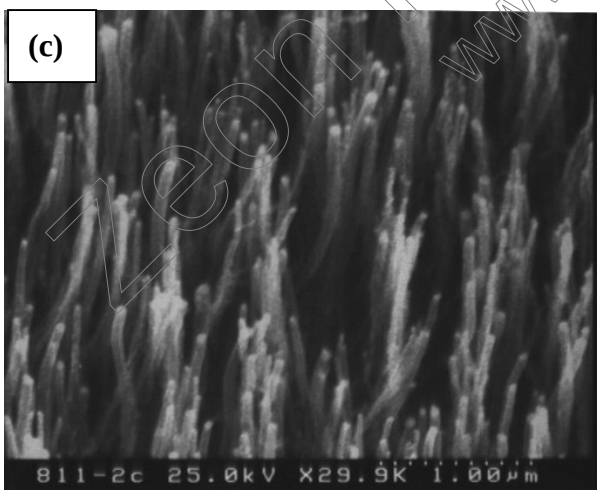

Specimen A3 (H_2/CH_4 : 20/10 sccm/sccm**)**

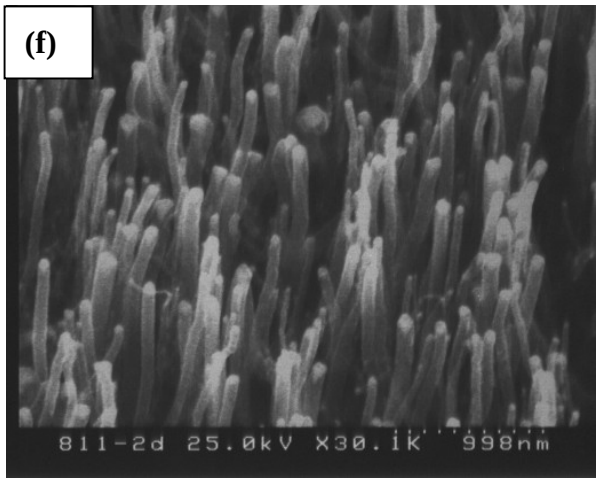

Specimen B3 (H_2/CH_4 : 20/10 sccm/sccm**)**

Fig. 4-2 The corresponding side view SEM images of Figs. 4-1.

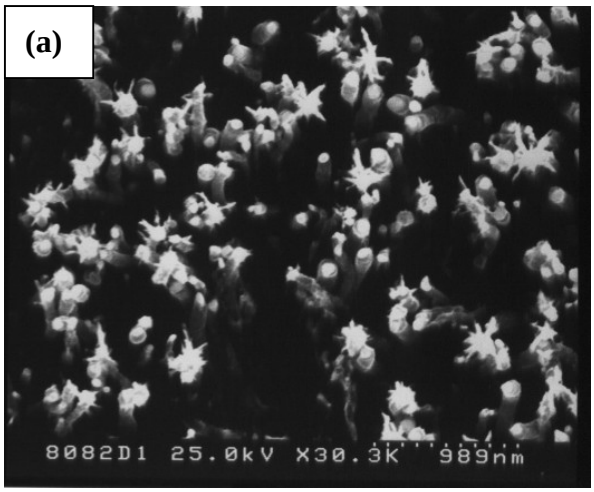

Top view (1 min H-plasma etching)

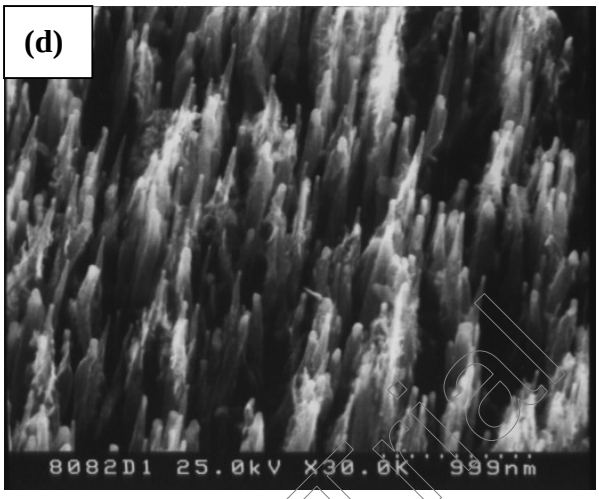

Side view (1 min H-plasma etching)

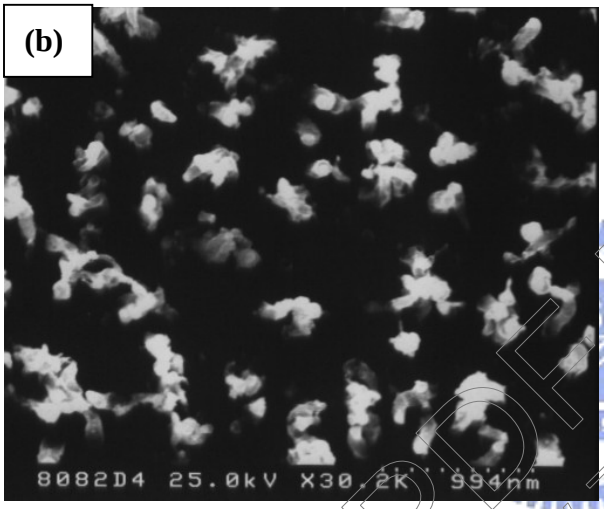

Top view (4 min H-plasma etching)

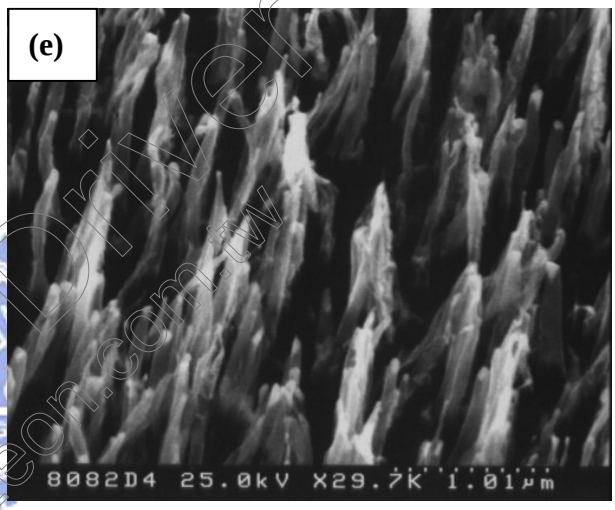

Side view (4 min H-plasma etching)

Top view (7 min H-plasma etching)

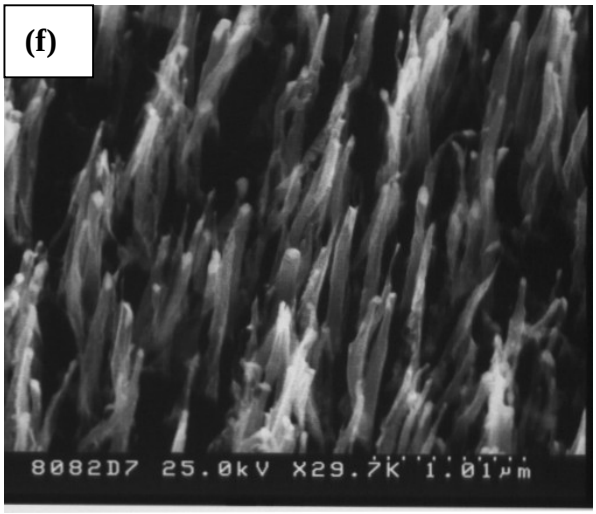

Side view (7 min H-plasma etching)

Figs. 4-3 Effect of H-plasma post-treatment on rattan-like CNTs morphology. (a), (b) and (c) are the top view SEM images of CNTs H-plasma post-treated for 1, 4 and 7 min (Con. 1, 4 and 5), respectively. (d), (e) and (f) are the corresponding side view of (a), (b) and (c), respectively.